昭和62年8月5日第三種郵便物許可　令和３年2月25日発行（隔月25日発行）　第39巻　第１号

MATERIAL TECHNOLOGY
材料技術

January-February
2021
Vol. 39, No. 1
ISSN 0289-7709
CODEN: MTECFQ

材料技術研究協会
Japan Research Institute of
Material Technology
https://www.jrimt.jp

MATERIAL
TECHNOLOGY
材料技術

VOL. 39, NO. 1
January-February

Contents

＜Articles＞

Decomposition of gaseous ethyl acetate with spherical pellets of Fe-Pt/Al_2O_3 catalyst using a combustion method

Mayuko TSUNASHIMA，Noriyuki KITAORI* ……1

Viscosity measurements of pseudoplastic cellulose nanofiber and polyethylene glycol water dispersions using optical tweezers

光ピンセットを用いた擬塑性を有するセルロースナノファイバー分散水およびポリエチレングリコール分散水の粘度測定

Daiki SUZUKI, Yuuki HOSOI, Naohiro Matsumoto, Kota NANRI, Toshiyuki SAITO and Hiroshi KINOSHITA

鈴木大輝，細井裕貴，松本直浩，南里浩太，齊藤利幸，木之下博 ……8

<Editorial Note>
On the occasion of the first on-line publication
材料技術誌のオンライン公開に寄せて ……14

Decomposition of gaseous ethyl acetate with spherical pellets of Fe-Pt/Al_2O_3 catalyst using a combustion method

Mayuko TSUNASHIMA[1)], Noriyuki KITAORI[1)*]

Abstract

The waste gases emitted from printing factories typically include volatile organic compounds (VOCs), such as ethyl acetate. In general, VOCs are decomposed by catalyst combustion methods, in which platinum catalysts are often employed. However, platinum is expensive and is a rare metal. In the present study, the development of an inexpensive iron-based catalyst was successfully achieved. The performance of the primitive iron catalyst was lower than the activity of commercially available platinum catalysts. Thus, a trace amount of platinum was added to the iron-based catalysts to improve the performance. Consequently, spherical pellets of the resulting Fe-Pt/Al_2O_3 catalyst exhibited optimal activity. Notably, the cost of the material was reduced by approximately 90%.

Keywords：Iron oxide, Spherical aluminum oxide, Combustion catalysts, VOCs, Platinum

Received September 5, 2020; accepted February 9, 2021

1) Department of Chemical Science and Engineering, Tokyo National College of Technology, Kunugida-machi, Hachiouji-shi, Tokyo, 193-0997, Japan

* E-mail: kitaori@tokyo-ct.ac.jp

1 Introduction

As a consequence of extensive use of various kinds of organic solvents, gases emitted by painting and printing factories often include large amounts of volatile organic compounds (VOCs).[1)] Exposure to VOCs, such as toluene and ethyl acetate, can have detrimental effects on people's health, and the emission of these chemicals typically produces unpleasant smells.[2-5)] For this reason, the concentrations of VOCs in industrial emissions are regulated by law, and all factories must conduct waste gas treatments to keep the levels of VOCs below the specified standard concentrations.[6-10)] Catalytic combustion methods are typically utilized in printing plants for VOCs treatment.[11-13)] A platinum-based catalyst in the presence of alumina as a carrier is generally employed due to its good oxidizing performance.[14,15)] However, it is widely known that platinum is a rare and relatively expensive metal. Accordingly, the fact that platinum accounts for a significant amount of material costs and leads to an increase in the price of the catalyst is a major issue.[16-18)] Therefore, the development of catalysts using inexpensive metal and metal oxides have been actively conducted.[19-23)] In this study, we attempted to reduce the cost of VOCs combustion catalysts by using iron. We selected iron instead of platinum due to availability and low cost. The performance of the iron-based catalyst was evaluated by investigating ethyl acetate gas decomposition reaction and comparing the activity with a commercially available platinum catalyst. The iron catalyst was prepared using a general impregnation method. Initially, the developed catalyst exhibited a lower decomposition performance than the platinum catalyst. Consequently, we examined a new method for the production of a different iron-based catalyst. This approach involved oxidizing iron by hydrogen peroxide, followed by its attachment to an alumina ball surface as FeOOH. The performance of the catalyst produced by this method was somewhat improved; however, remained lower than that of the platinum catalyst. Since inadequate catalyst performance was obtained using just iron, further improvements were necessary. We subsequently investigated addition of a small amount of platinum to the iron catalyst. Ultimately, the performance of the catalyst-containing platinum exhibited activity equivalent to that of a commercially available platinum catalyst and importantly, the cost of the material was significantly reduced.

2 Experimental

2.1 Preparation of the iron-based catalyst

Fig. 1 shows the photographs of visual appearance of the iron-oxide catalyst and the iron-oxyhydroxide catalyst. The iron catalysts were prepared using two varying approaches. The first included the synthesis of the iron-based catalyst using a previously described impregnation method.[24)] Spherical aluminum oxide with a diameter of 5 mm was used as a catalyst carrier (Nikki-Universal Co.). The carriers (alumina balls) were immersed in a $FeSO_4$ solution whose concentration is 4.9wt.% and 11.7wt.% for 5 min. Subsequently, the carriers were dried at 100 °C in a dryer and baked at 500 °C in air, affording the desired iron-oxide catalysts (see Fig. 1a). The catalysts were prepared using two different a $FeSO_4$ solution concentrations, i.e., 4.9wt.% and 11.7wt.%.

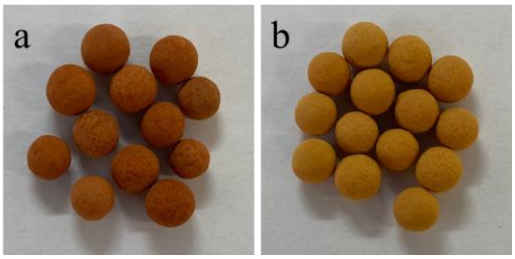

Fig. 1 The visual appearances of the iron-oxide catalyst (a) and the iron-oxyhydroxide catalyst(b)

In the second approach, the alumina balls were immersed in a $FeSO_4$ solution, to which hydrogen peroxide was added. The ionic iron species were oxidized by hydrogen peroxide to form iron compound on the surface of the alumina ball. Following oxidation, the carriers were dried at 100 °C in a dryer (see Fig. 1b). The X-ray diffraction (XRD) pattern of iron compound on the catalyst surface was recorded by the X-ray diffractometer (D8-Advance, Bruker). In addition, infrared (IR) spectra of iron compounds on the catalyst surface were recorded using the Fourier transformation infrared spectrophotometer (FT/IR-4100typeA, Jasco). The measured sample was prepared by scraping the outer surface of catalysts.

Furthermore, the catalysts were prepared by the addition of a small amount of platinum to the as-synthesized iron catalysts. The two types iron

catalysts were immersed in a 0.1 g/L dinitrodiamine platinum nitrate solution (Tanaka Kikinzoku Kogyo, Japan) for 1 h. This resulted in the fixation of the majority of the platinum species in the solution to the catalysts. It is noteworthy that the platinum solution concentration was 20-fold lower than the amount of platinum required to produce a commercial catalyst (Nikki-Universal Co.). The commercially available platinum catalyst was evaluated using X-ray fluorescence analysis (Shimazu corporation, EDX-7000). It was found that approximately 1.7–2.2 g of platinum was attached to 1 L of the carrier. Subsequently, the immersed catalysts were dried at approximately 100 °C in a dryer, affording two types of Fe-Pt composite catalysts.

2.2 Evaluation of the catalytic activity

The evaluation of the catalyst performance for oxidative decomposition of gaseous VOCs was carried out using ethyl acetate gas at a concentration of 5000 ppm. The fixed bed reactor was used for the evaluation. The ethyl acetate gas was passed through a catalyst-containing heated furnace at a flow rate of 3 L/min. The air before and after passing through the catalyst was analyzed by gas chromatography (GC). The activity of a commercially available platinum catalyst, i.e., the standard for the catalytic performance, was assessed utilizing the same experimental system. The catalyst performance evaluation system is illustrated in Fig. 2. All piping consisted of silicone hoses. The air drawn by the

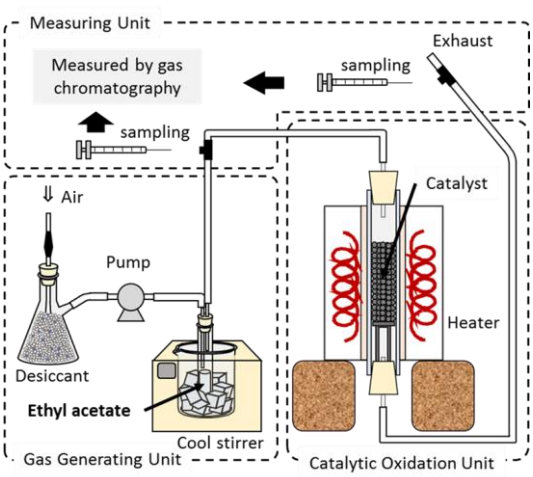

Fig. 2 The fixed bed reactor system for evaluation of catalytic activity

pump was passed through silica gel to produce dry air exhibiting the relative humidity of 2–5%. A test gas mixture of air and ethyl acetate at a concentration of 5000 ppm was prepared by blowing dry air onto ethyl acetate in a test tube. The catalyst with height of 20 cm was in the quartz tube (a diameter of 26 mm and length of 500 mm.), which was heated using a ring furnace. The space velocity was approximately 424 /hr in the evaluation. The ethyl acetate gas was passed through the heated catalyst in the quartz tube from top to bottom. After passing through the sample, the gas was exhausted and analyzed by GC. The catalysts were heated at a temperature in the range of 250–400 °C. The concentration of gas was analyzed 5 times with the one temperature. The composition and specific surface area of the catalysts were measured by X-ray fluorescence analysis as well as using Brunauer-Emmett-Teller (BET) methods, respectively. Lastly, the surface structures were observed by scanning electron microscopy (SEM).

3 Result and discussion

3.1 Performance of the iron-oxide catalysts

The iron elemental content in the iron-oxide catalysts was measured by X-ray fluorescence analysis. We determined that the iron elemental content using the 11.7% $FeSO_4$ solution was 0.441 mg/cm^2, while the iron elemental content utilizing the 4.9% $FeSO_4$ solution was 0.245 mg/cm^2. The catalytic performance of the iron-oxide catalysts under the oxidation conditions is shown in Table 1. The ethyl acetate concentration after passing the catalyst is a mean value of 5 times analyzes. The catalyst activity was evaluated at 300 °C, 350 °C, and 400 °C. Examination of the gas after passing through the iron catalyst with the content of 0.441 mg/cm^2 revealed that 1905 ppm of ethyl acetate was detected at 300 °C, while at 350 °C, 70 ppm of the compound was noted. It is noteworthy that no ethyl acetate was detected at 400 °C; therefore, complete decomposition was suspected. Moreover, analysis of

Table 1 Characteristics of the Fe/Al_2O_3 catalyst

Supported amount of Fe(mg/cm^2)	Oxidation method	Ethyl acetate concentration after passing the catalyst(ppm)		
		Treatment temperature(°C)		
		300	350	400
0.441	Baking at 500°C	1905	70	0
0.245		2775	23	0
0.445	Addition of H_2O_2	456	0	0
0.270		487	63	0
Commercial platinum catalyst		0	0	0

the gas after passing through the iron catalyst with the content of 0.245 mg/cm^2 showed that 2775 ppm of ethyl acetate was noted at 300 °C, 23 ppm at 350 °C, and 2 ppm at 400 °C. Thus, the decomposition performance of ethyl acetate increased with increasing furnace temperature. In addition, the activity of the iron catalyst deposited with the content of 0.441 mg/cm^2 to decompose ethyl acetate was higher than that at the catalyst with the content of 0.245 mg/cm^2. Hence, we established that during the decomposition of ethyl acetate, the performance of the catalyst was enhanced with an increase in the iron content.

It was determined that the commercially available platinum catalyst completely decomposed ethyl acetate at 300 °C. On the other hand, iron catalysts require a temperature of 400 °C or higher. To improve the performance of the iron catalyst, we attempted to alter the method of oxidizing iron.

3.2 Changes in the catalytic activity following hydrogen peroxide oxidation

The performance of the iron catalyst, in which the iron was oxidized using hydrogen peroxide to produce iron oxyhydroxide on the catalyst surface is shown in Table 1. To compare the performance of the iron-oxyhydroxide catalyst with the iron-oxide catalyst, a sample of the former was prepared, and the amount of supported iron was measured by X-ray fluorescence analysis. It was found that the amount of iron in both types of catalysts was nearly the same. When the content of the iron element was 0.445 mg/cm^2, 456 ppm of ethyl acetate was detected after passing through catalysts at 300 °C. No ethyl acetate was detected at 350 °C or 400 °C. When the deposition amount of iron on the catalyst surface was at 0.270 mg/cm^2, 487 ppm of ethyl acetate was detected at 300 °C, whereas at 350 °C, 63 ppm was noted. Moreover, at 400 °C, no ethyl acetate was detected. Similarly to the case of iron-oxide catalysts, the decomposition of ethyl acetate increased with increasing the processing temperature of the electric furnace. In addition, the catalyst oxidation capacity of ethyl acetate improved with increasing iron content. The comparison of the performance of iron catalysts prepared using two different oxidation methods revealed that the activity of the catalyst oxidized employing hydrogen peroxide was superior.

According to Fig. 2b, the iron compound prepared by the second approach is yellowish brown.[25-28] For that reason, this iron compound is considered FeOOH. Fig. 3 shows the XRD pattern of iron compound on the catalyst surface. It is considered the amorphous peaks at 2θ = 35.3°, 36° originated from δ-FeOOH and β-FeOOH.[29,30] Fig. 4 shows the IR spectra of the iron compound on the catalyst surface. Two absorption band observed around 705 and 847 cm^{-1} originated from β-FeOOH.[33] Furthermore, an absorption band observed around 1125 cm^{-1} originated from δ-FeOOH.[34] Considering these results from XRD pattern and IR spectra, the iron compound on the catalyst surface is identified the mixture of δ-FeOOH and β-FeOOH. When heated above 250 °C, iron oxyhydroxide (FeOOH) finally converts to iron oxide; therefore, heating does not change the iron content. However, the structure of the catalyst surface was altered by thermal decomposition of iron oxyhydroxide.

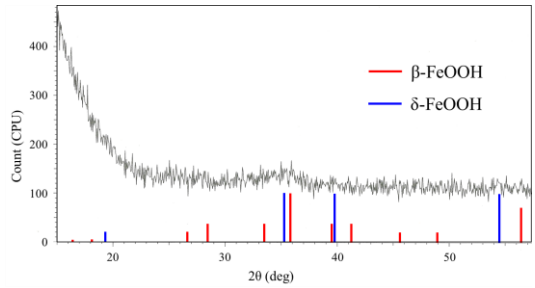

Fig. 3 X-ray diffraction pattern of the Fe compound coated on the iron-oxyhydroxide catalyst surface

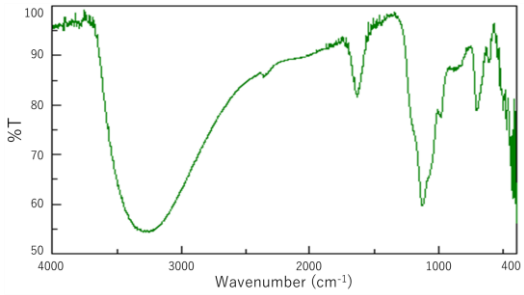

Fig. 4 The infrared spectra of the Fe compound coated on the iron-oxyhydroxide catalyst surface

The SEM images of the two types of iron catalyst surfaces are illustrated in Fig. 5. Based on the SEM observation, the surface of the iron catalyst formed by baking at 500 °C was flat, while the surface of the iron catalyst oxidized with hydrogen peroxide was composed of numerous fine particles of approximately 0.1~0.5 μm and many pores of 1 μm.

To gain further insight, we subsequently

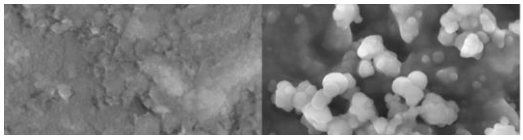

Table 2 Characteristics of the Fe-Pt/Al_2O_3 catalyst

Supported amount of Fe (mg/cm²)	Oxidation method	Ethyl acetate concentration after passing the catalyst (ppm)		
		Treatment temperature (℃)		
		250	300	350
0.441	Baking at 500℃	1	0	0
0.245		Not measured	60	0
0.445	Addition of H_2O_2	0	0	0
0.270		0	0	0
Commercial platinum catalyst		5	0	0

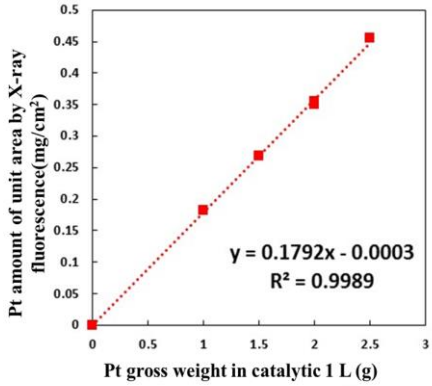

Fig. 6 Relationship between the platinum amount per unit area measured by X-ray fluorescence analysis and the gross platinum mass attached to 1 L of alumina pellets

measured the BET specific surface area of the catalysts. The specific surface area of the carriers (alumina balls) was 141 m^2/g. And the specific surface area of the heat-oxidized iron catalyst was established at 145 m^2/g, whereas the specific surface area of the iron catalyst oxidized with hydrogen peroxide was 171 m^2/g. These results were consistent with the SEM observation. Thus, it is considered that the iron catalyst prepared from oxyhydroxide exhibited a large specific surface area, and thus the dispersion effect is high, which is an advantageous property for catalytic reactions.[35-37] Furthermore Because of having many pores, contact efficiency between the iron catalyst oxidized with hydrogen peroxide and reaction gas increased. Thus, it is considered that the catalyst performance has improved.[38,39]

3.3 Improvement of the iron catalyst performance by the addition of trace platinum

The Fe-Pt catalysts were obtained by adding a small amount of platinum to the two types of iron catalysts. The performance of the prepared catalysts is shown in Table 2.

It was found that the Fe-Pt catalysts (impregnation method) prepared by the addition of trace platinum completely decomposed ethyl acetate at 300 °C (high iron content catalyst) and at 350 °C (low iron content catalyst). Furthermore, the Fe-Pt catalyst obtained by adding trace platinum to the iron-oxyhydroxide catalyst decomposed ethyl acetate at 250 °C, regardless of the Iron content. Notably, the performance of this Fe-Pt catalyst was shown to outperform the characteristics of commercially available platinum catalysts. Moreover, the Fe-Pt catalyst prepared by the addition of platinum to the iron-oxide catalyst containing a large supported amount as well as the catalyst obtained by adding platinum to the iron-oxyhydroxide catalyst exhibited analogous performance to the commercially available platinum catalyst. We suspect that this is a consequence of the addition of a small amount of platinum to the iron catalyst, which promoted the catalytic activity of iron. Platinum is known to display strong dehydrogenating effects on hydrocarbon molecules.[40] Thus, the presence of platinum results in dehydrogenation and activation of ethyl acetate. Subsequently, iron catalyzes the decomposition of ethyl acetate activated by platinum. Therefore, it is considered that the decomposition proceeds more easily using both catalysts than with iron alone. The amount of the supported platinum was also measured by X-ray fluorescence analysis. We determined that the platinum content of the commercially available platinum catalyst was 0.333 mg/cm^2, while the platinum content of the Fe-Pt catalyst was in the

range of 0.014–0.016 mg/cm^2.

The relationship between the platinum amount per unit area measured by X-ray fluorescence analysis and the total platinum mass attached to 1 L of spherical alumina pellets is demonstrated in Fig. 6. As it can be seen, the platinum content in the Fe-Pt catalyst at 0.014–0.016 mg/cm^2 corresponds to approximately 0.1 g of platinum attached to 1 L of the alumina pellets. Furthermore, the platinum content of this Fe-Pt catalyst is approximately 1/20 that of a commercially available platinum catalyst, the catalytic performance is enhanced. Importantly, the material costs were reduced by approximately 90%. Based on the results of our study, the cost of the combustion catalyst was significantly reduced by utilizing the described catalytic system consisting of iron and trace platinum.

4. Conclusion

The performance of the developed iron-based catalysts was evaluated using ethyl acetate gas decomposition reaction and compared with a commercially available platinum catalyst. The activity of the iron-oxide catalyst obtained utilizing a general impregnation method was lower than that of the commercially available platinum catalyst. Based on this result, we searched for a new approach for producing a more efficient iron catalyst. The iron was oxidized by hydrogen peroxide and attached to an alumina surface as FeOOH. The performance of the iron-oxyhydroxide catalyst prepared in this way considerably improved; however, it was not as high as the activity of commercially available platinum catalysts. Since the catalyst performance using just iron was inadequate, it was necessary to make further improvements. Hence, we prepared Fe-Pt catalysts by the addition of a very small amount of platinum to the iron catalysts. As a result, it was found that the catalyst performance was enhanced to the level of commercially available platinum. Ultimately, the mass of platinum used was reduced to approximately 1/20 of that of commercially available platinum catalysts, and the overall cost of the VOCs decomposition and combustion catalysts was greatly reduced.

References

1) G. Li, W. Wei, X. Shao, L. Nie, H. Wang, X. Yan and R. Zhang, *Journal of Environmental Sciences*, **2018,** *67*, 78-88.
2) M. Kampa and E. *Castanas, Environmental Pollution*, **2008,** *151*, 362-367.
3) J. S. Kiurski, B. B. Marić, S. M. Aksentijević, I. B. Oros, V. S. Kecić, and I. M. Kovačević, *Renewable and Sustainable Energy Reviews*,**2013,** *28*, 224-231.
4) K. Jelena, M. Branislav, A. Dragan, M. Aleksandra, G. Selena, O. Ivana, and K. Jelena, *Renewable and Sustainable Energy Reviews*, **2012,** *16*, 660-667.
5) D. Ye, M. Klein, H. H. Chang, J. A. Sarnat, J. A. Mulholland, E. S. Edgerton, A. Winquist, P. E. Tolbert, and S. E. Sarnata, *Epidemiology*, **2017,** *28*, 197-206.
6) Y. Nishimura, *The Surface Finishing Society of Japan*, **2005,** *56*, 594-600 . [in Japanese]
7) Y. Yonehara, *Japan Society of Colour Material*, **2017,** *90*, 122-126. [in Japanese]
8) W. H. Cheng, S. K. Hsu, M. S. Chou, *Journal of Environmental Management*, **2008,** *88*,1485-1494.
9) D. F. Zhao, A. Buchholz, R. Tillmann, E. Kleist, C. Wu, F. Rubach, A. Kiendler-Scharr, Y. Rudich, J. Wildt and Th. F. Mentel, *Nature Communications*, **2017,** *8*, Article number: 14067.
10) K. Taguchi, J. *Japan Association on Odor Environment*, **2004,** *35*, 135-138. [in Japanese]
11) W. B. Li, J. X. Wang, and H. Gong, *Catalysis Today*, **2009,** *148*, 81-87.
12) F. N. Aguero, B. P. Barbero, L. Gambaro, and L. E. Cadu´ s, *Applied Catalysis B: Environmental*, **2009,** *91*, 108-112.
13) D. Delimaris and T. Ioannides, *Applied Catalysis B: Environmental*, **2008,** *84*, 303-312.
14) T. Muroi, *Materia Japan*, **2001,** *40*, 206-209. [in Japanese]
15) S. Somekawa, T. Hagiwara, K. Fujii, M. Kojima, T. Shinoda, K. Takanabe, and K. Domen, *Applied Catalysis A: General*, **2011,** *409-410*, 209-214.
16) M. S. Kamal, S. A. Razzak and M. M. Hossain, *Atmospheric Environment*, **2016,** *140*, 117-134.
17) X. H. Tai, C. W. Lai, J. C. Juan and K, M, Lee, *Nanomaterials for Air Remediation, Micro and Nano Technologies*, **2020,** Chap. 7.
18) Clariant Corporation. Z. Dang, G. Cullen. LOW COST OXDATION CATALYSIS FOR VOC AND HALOGENATED VOC EMISSION CONTROL, U. S. patent 10,569,256. 2020-2-25.
19) D. A. Aguilera, A. Perez, R. Molina and S. Moreno, *Applied Catalysis B: Environmental*, **2011,** *104*, 144-150.

20) M. H. Castano, R. Molina, S. Moreno, *Molecular Catalysis*, **2017**, *443*, 117-124.
21) D. Delinaris, T. Loannides, *Applied Catalysis B: Environmental*, **2009,** *89*, 295-302.
22) X. Yang, X. Yu, M. Lin, X. Ma, M. Ge, *Catalysis Today*, **2019,** *327*, 254-261.
23) S. Dissanayake, N. Wasalathanthri, A. S. Amin, J. He, S. Poges, D. Tathnayake, S. L. Suib, *Applied Catalysis A: General*, **2020,** *590* Article number: 117366.
24) Y. Morioka, S. Okada, H. Kosugi, and J. Kobayashi, *The Chemical Society of Japan*, **1989,** *4*,653-659 (1989). [in Japanese]
25) A. Jagminas, K. Mazeika, J.Teklaitis, D. Baltrunas, *Applied Surface Science*, **2010**, *256*, 3993-3996.
26) R. B. Pujari, S. J. Patil, J. Park, A. Shanmugasundaram, *Journal of Power Sources*, **2019**, *436*, 226826.
27) R. Yu, J. Pee, Y. J. Kim, *Journal of Nanoscience and Nanotechnology*, **2013**, *13*, 1-3.
28) X. Chen, Y. Jiang, C. Jiao, *Journal of Hazardous Materials*, **2014**, *266*, 114-121.
29) JCPDS ASTM Cards No. 13-87.
30) JCPDS ASTM Cards No. 18-639.
31) S. Nobuoka, T. Ando, *Science of powder*, **1966**, *13*, 286-289. [in Japanese]
32) S. Nobuoka, *The journal of chemical industry*, **1965**, 68, 2311-2317. [in Japanese]
33) K. Sato, T. Koike, M. Aoki, *Japan Analyst*, **1972**, *21*, 256-263. [in Japanese]
34) T. Misawa, W. Suetaka, S. Shimodaira, *Journal of the Society of Materials Science, Japan*, **1970**, *19*,537-542. [in Japanese]
35) A. T. Bell, *Science*, **2003,** *299*, 1688-1691.
36) J. C. S. Wu, Z. A. Lin, J. W. Pan, M. H Rei, *Applied Catalysis A: General*, **2001,** *219*, 117-124.
37) M. Morbidelli, A. Gavriilidis, A. Varma, *Catalyst Design: Optimal Distribution of Catalyst in Pellets, Reactors, and Membranes*, **2001,** *Cambridge University Press*, 40-46.
38) R. Portela, V. E. Garcia-Sanchz, M. Villarroel, S. B. Rasmussen, P. Avila, *Applied Catalysis A: General*,**2016,** *510*, 49-56.
39) Q. -H. Xia, K. Hidajat, S. Kawai, *Ctalysis Today*, **2001,** *68*, 255-262 (2001).
40) E. Kikuti, Y. Imizu, K. Segawa, A. Tada, and H. Hattori, *Shinpan Atarashishokubaikagaku*, **2013,** *Sankyo Shuppan*, Tokyo, Chap. 1. [in Japanese]
41) L. Xinsheng, K. Olga, F. Robert, *Applied Catalysis A: General*, **2002**, *226*, 293-303.
42) L. Lingling, M. Chenfang, W. Shaohuang, Y. Shaoming, C. Feng, Y. Chenqing, Z. Huanglong, Y. Donghong, *Journal of Electroanalytical Chemistry*, **2020**, *877*, 114519.
43) C. Wei, K. Jaemin, S. Shouheng, C. Shaowei, *The Journal of Physical Chemistry C*, **2008**, *112*, 3891-3898.

光ピンセットを用いた擬塑性を有するセルロースナノファイバー分散水およびポリエチレングリコール分散水の粘度測定

鈴木　大輝 [1)],　細井　裕貴 [1)], 松本　直浩 [1)],　南里　浩太 [2)],　齊藤　利幸 [2)],
木之下　博 [1)*]

Viscosity measurements of pseudoplastic cellulose nanofiber and polyethylene glycol water dispersions using optical tweezers

Daiki SUZUKI[1)], Yuuki HOSOI[1)], Naohiro Matsumoto[1)], Kota NANRI[2)], Toshiyuki SAITO[2)] and Hiroshi KINOSHITA[1)]

Abstract

We previously have reported that optical tweezers can measure drag forces in liquids in micrometer regions. Viscosities of liquids can also be calculated from the drag forces. Liquids, in which nanomaterials and polymers are dispersed, often exhibit pseudoplasticity. The viscosities of the pseudoplastic fluids increases with decreasing shear rates. Since a shear rate of optical tweezers is very slow, it is presumed that the measured viscosities using optical tweezers are larger than those of conventional viscosity measurement methods. Moreover, aggregations of nanomaterials and polymers would cause non-uniformity of viscosity in micrometer regions. However, they have been not measured. In this study, viscosities of a cellulose nanofiber (CNF) water dispersion and a polyethylene glycol (PEG) water dispersion, which show pseudoplasticity, were measured by an optical tweezers. Measured viscosities of the pseudoplastic fluids using the optical tweezers decreased with increasing the shear rates, which phenomenon is peculiar to pseudoplastic fluids. The measured viscosities were larger than those of a conventional viscosity measurement method. Moreover, non-uniformity of viscosities in micrometer regions were measured and the difference of the viscosities between the CNF and PEG water dispersions, which would arise from the difference of the structures of CNF and PEG, was observed. These results indicate that optical tweezers can measure viscosities of pseudoplastic fluids in micrometer regions.

KEYWORDS：optical tweezers, viscosity, micro-range, cellulose nanofiber, polyethylene glycol

Received January 4, 2021; accepted March 19, 2021

---

1) School of Engineering & Graduate School of Engineering, University of Hyogo, Himeji, Hyogo 671-2280, Japan
2) R&D Department, JTEKT CORPORATION, Kariya, Aichi 448-0803, Japan

1) 兵庫県立大学大学院工学研究科，〒671-2280　兵庫県姫路市書写 2167
2) 株式会社ジェイテクト研究開発本部，〒448-0803　愛知県刈谷市野田町北地蔵 1-7

*E-mail: kinoshita@eng.u-hyogo.ac.jp

１．はじめに

ナノ材料や高分子などを液体に分散させると，これらが液中で抵抗となって液体の粘度が大きくなる [1, 2]。ただそれらの粘度は単純に分散したナノ材料や高分子の密度や濃度に依存するものではない。これは，ナノ材料や高分子は分散液体中でファンデルワールス力や水素結合などで結合し，三次元的な網目構造 [3]などを形成する場合もあるからである。これら網目構造はせん断を加えると結合が切れて粘度が低下し，せん断速度が速いほど粘度が低下する擬塑性を示すことも多い [1, 2]。

さらに液中での凝集によってナノ材料や高分子の濃度が高いところでは粘度が高く，濃度が低いところでは粘度が低くなるなど，ミクロで見ると粘度も不均一となっている可能性がある。しかしながらこれまでの粘度測定法では少なくとも数 ml の容量が必要であり，測定される粘度はこれらの平均化された値で，微小領域での粘度の不均一性は，これまで調べられたことがない。

微小領域での粘度を調べることは，微小領域での液体の流動特性を把握するために非常に重要である。例えば摩擦界面では，潤滑液体は摩擦する二つの平面によって数 nm から数十 μm の狭い領域に閉じ込められている。また潤滑液体の性能を向上させるため近年では金属ナノ粒子 [4], カーボンナノ材料 [5–7]といったナノ材料を潤滑液体に分散する研究がなされている。摩擦下の狭い領域でのナノ材料が分散された潤滑液体では粘度が不均一あるいは通常の方法で測定した値とは異なる可能性がある。また最近研究されているドラッグデリバリーシステムでは，薬を運ぶ役割としてナノ材料 [8]や高分子 [9]が研究されており，これらが分散された血液の血管内での流動特性を見積もるためにも粘度を知る必要がある。さらに精子 [10]あるいは高分子 [11]をマイクロ流路に流れる液体に分散して，流れを利用してこれらを濾過する研究が開発されてきているが，これらのマイクロ流路内での粘度は測定されていない。

前報で光ピンセットによる力学的な計測技術の検討により, 分散水の低 Reynolds 数領域において抗力の測定が可能なことを報告した [12]。光ピンセットでは測定する液体に直径が数十 μm の微粒子を分散させ，集光したレーザー光でこの微粒子をトラップする。それから液体を移動させると，微粒子に抗力が加わり，その分だけ静止位置から変位する。この変位量を測定することで抗力を計算でき，さらに液体の粘度も見積もることができる。それゆえ光ピンセットでは，数十 μm の領域で粘度測定を行うことができる。ただ，ナノ材料が分散された液体の粘度測定の場合，多くの材料で擬塑性が現れるが [3]，光ピンセットでのせん断速度は最大でも数十 μm/s 程度であり，そのような非常に遅いせん断速度での粘度測定値は未明である。

そこで本研究ではナノ材料としてセルロースナノファイバー(cellulose nanofiber; CNF)とさらに高分子としてポリエチレングリコール(polyethylene glycol; PEG)を用い, これらを水に分散した分散水について光ピンセットで微小領域の粘度測定を行った。CNF は水に分散すると擬塑性を [1]，さらに PEG も分散水中では，やはり擬塑性を示すことが報告されている [13]。また CNF と PEG はそれらの分散水が透明であり，レーザー光を透過させる必要のある光ピンセット測定に適した材料であり，本研究では両者を選択した。また光ピンセットでの粘度測定に加えてこれらの分散水を一般的な粘度測定法であるキャノン・フェンスケ粘度測定法でも測定し，両者の測定法で結果を比較した。

2.　実験装置および実験方法

2.1　実験装置

Figure 1 に本実験で用いた光ピンセット装置の概要を示す。基本的に前報で説明した装置構成と同一であるが [12]，トラップ粒子の変位量測定を前報では四分割のフォトダイオードを用いたが，本実験では CCD カメラから得た画像

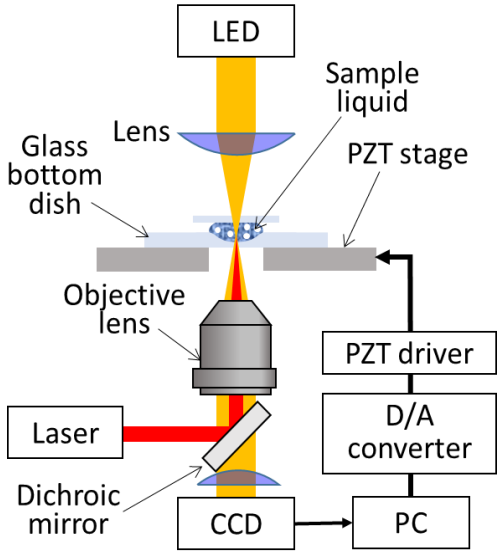

Fig 1. Schematic of optical tweezers system used in this study

を解析することで行っている。微粒子をトラップするために波長 975nm の半導体レーザー光（光源 Thorabs 製 BL976-SAG300）を出力する。レーザー光は最終的に倍率 100 倍の対物レンズを通して集光する。またレーザー光の入射方向と反対側から微粒子観察用の白色 LED 光を照射している。観察用の CCD カメラ（Thorabs 製 DCC1240C-HQ）の観察方向は入射レーザー光と同方向であり，ダイクロイックミラーを通して光路を分離し観察している。CCD カメラによって撮影された映像は，コンピュータで確認でき，さらに動画を保存できる。

試料液体は深さ 1mm のボトムディッシュの凹部とカバーガラスの間に納められている。このボトムディッシュはピエゾ素子によって X-Y-Z 方向に移動が可能で，試料液体を任意方向に任意速度で移動できる。

2.2　粘度算出方法

前報で説明したように，光ピンセットのレーザー光でトラップした液体中の微粒子は液体を移動させると，液体の抗力 F_η[N]によって微粒子がトラップ中心から変位する [12]. この変位量を d_x[mm]，トラップ力によるばね定数を k[N/m]とすると次の関係が得られる。

$$F_\eta = k\, d_x \qquad (1)$$

ばね定数 k はトラップ微粒子のブラウン運動から求められる [12]。さらに粘度 η[Pa・s]の液体中を移動する微粒子が受ける抗力は，微粒子半径を a[mm]，微粒子移動速度を v[mm/s]とすると次の式から求められる。

$$F_\eta = 6 \cdot \pi \cdot a \cdot \eta \cdot v \qquad (2)$$

すなわち d_x を測定することにより(1)式と(2)式から液体の粘度を計算できる。微粒子のずれ量は，微粒子を左右に幅 10μm で合計 5 回移動させたときの，各々の往復の右側のずれ量と左側のずれ量を平均している。

今回の実験では一般的な粘度測定法として精度が高いキャノン･フェンスケ粘度計(柴田科学㈱)を用いて粘度測定し比較した。またキャノン・フェンスケ粘度計で測定した動粘度から粘度を求める際に液体の密度が必要になる。そのため，CNF と PEG を分散せた試料分散水の正確な密度は，標準比重計(アズワン㈱)を使用して測定した。

2.3　試料

実験に用いた CNF(第一工業製薬製レオクリスタ I-2SX)は，原料パルプを TEMPO(（2,2,6,6-テトラメチルピペリジン 1- オキシル)酸化処理でセルロースを解繊し，さらに機械的なナノ分散処理を行ったものであり，シングルサイズとなっている [1]。PEG(富士フィルム和光純薬)は式量が 8000 のものを用いた。CNF 分散水は CNF 濃度が 0.02-0.10mass%の間で，また PEG 分散水については PEG 濃度が 2-10mass%の間で精製水に分散させて用いた。今回，全ての試験においてトラップする微粒子として SiO_2 粒子(AGC エスアイテック㈱)を使用した。微粒子径は CCD カメラの画像から測定したが，すべて約 4μm の直径であった。

3. 実験結果と考察

Figure 2 は CNF 濃度が 0.02mass%から 0.10mass%，微粒子移動速度が 2.3μm/s から 6.7μm/s で測定した時の CNF 分散水の粘度をまとめたものである。CNF 濃度が 0.10mass%を超える時は粘度が大きすぎて，今回の装置では微粒子を移動できず粘度を測定できなかった。測定は異なる 3 つの微粒子で，さらに 5 箇所の異なる場所で測定を行い，それら 15 回の異なる場所での測定を平均しグラフに示している。同じ粒子移動速度では CNF 分散水の濃度が高いほど大きな粘度となっている。CNF 分散水の濃度が 0.05 mass%以下では粒子移動速度を変化させても粘度はほぼ変化なく一定であることが分かる。しかし CNF 濃度が 0.06 mass%以上の時，CNF 分散水の粘度は粒子移動速度が速くなるほど低下している。

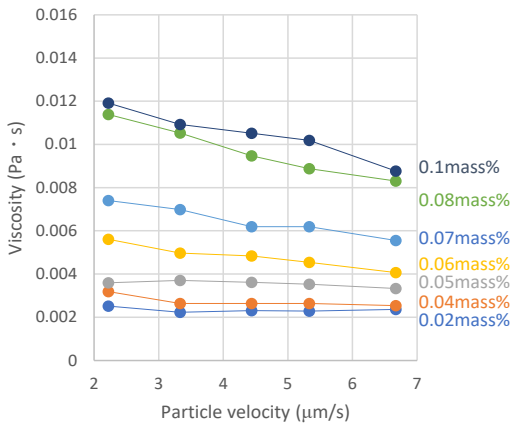

Fig 2. Viscosities of the CNF water dispersions as a function of the particle velocity with the CNF concentrations between 0.02 and 0.1 mass%.

CNF は酸素官能基を有し，分散水中で各々 CNF が水素結合で結合し網目構造を形成してゲル状の水分散体を形成する [14]。これが抵抗となって粘度が増加する [1]。ただし、せん断を加えると網目構造が破壊され粘度が低下する。これが，CNF 分散水が擬塑性を示す理由と考えられる。光ピンセットでの粒子移動速度はせん断速度と同様に考えられるため，光ピンセットでの粘度測定で濃度が高いときの微粒子速度増加に伴う粘度減少は同様にせん断によって CNF 間の水素結合を切断し網目構造を破壊して，粘度が低下していると思われる。つまり光ピンセットによる非常に遅いせん断速度，さらにミクロな領域の測定でも擬塑性流体特有の現象を測定できることが明らかとなった。

Figure 3 は Figure 2 に示した光ピンセットで測定した微粒子移動速度が 2.2μm/s の時(2.2μm/s OP)と 6.7μm/s(6.7μm/s OP)時の結果を，横軸を濃度，縦軸を粘度としたもので，さらにキャノン・フェンスケ粘度計により測定した粘度(CF)を加えている。この図のエラーバーは 15 回の測定で最小値，最大値を示している。先ほど説明したように，濃度が同じ時は光ピンセットで測定した値は微粒子移動速度が小さい方が大きくなっている。濃度の増加に伴い，光ピンセットで測定した値，およびキャノン・フェンスケ粘度計で測定した粘度共に増加している。また光ピンセットで測定した粘度は微粒子移動速度が速い時でもキャノン・フェンスケ粘度計で測定した値よりも高く，濃度が高くなるにつれて，その差が大きくなっている。キャノン・フェンスケ粘度計では液体の細管内での落

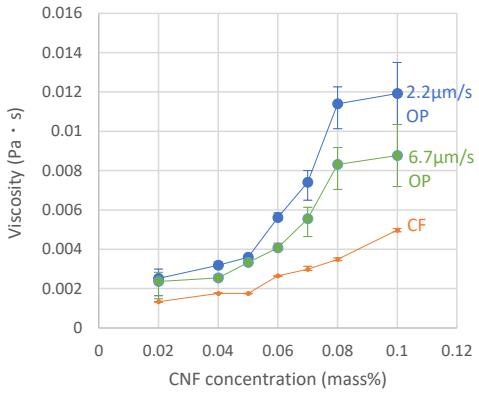

Fig 3. Viscosities of the CNF water dispersions as a function of the CNF concentrations measured by the optical tweezers at the particle velocity of 2.2 and 6.7 μm/s, and the Cannon-Fenske viscometer.

下速度を測定することで粘度を計算しており，その落下速度は約 7.2 cm/s なので光ピンセットよりもかなり速く，低い粘度で測定されたと考えられる。

また光ピンセットで測定した粘度では，エラーバーの幅が高濃度になるほど大きくなっており，さらにこの幅は微粒子移動速度に依存せず, CNF 濃度が同じであればほぼ同じであった。これに対してキャノン・フェンスケ粘度計での測定ではエラーバーが平均値を示す丸に隠れるほど値が小さく一定している。キャノン・フェンスケ粘度計では数十 ml の液体の平均値となっている。対して光ピンセットでは 20μm の範囲の極微小領域で粘度を測定している。それゆえエラーバーの幅が大きくなった理由として, CNF 分散液中の粘度がミクロで見ると不均一であると考えられる。これは CNF のゲル状の水分散体の濃度が，光ピンセットの微小領域測定で認識できる範囲で不均一である可能性がある。

Figure 4 は PEG 濃度が 2 mass%から 10 mass%, 微粒子移動速度が 2.3 μm/s から 6.7 μm/s で変化させて測定した時の粘度をまとめたものである。PEG 濃度が 10 mass%を超えると粘度が高すぎて測定できなかった。また 2 mass%以下の濃度では精製水と変わらない濃度であった。このように CNF 分散水よりもかなり高い濃度で測定を行った。またグラフの値は CNF と同様に異なる場所での 15 回の測定を平均した値である。CNF と同様に同じ粒子移動速度では PEG 分散水の濃度が高いほど大きな粘度となっている。PEG 分散水の濃度が 5 mass%以下では粒子移動速度によらず粘度はほぼ一定であることが分かる。しかし PEG 濃度が 8 mass%以上の時，CNF 分散水と同様に PEG 分散水の粘度は粒子移動速度が速くなるほど粘度が低下している。PEG は水溶液中で，水素結合によって会合し，これらが抵抗となって粘度が増加すると報告されている [15]。それゆえ，せん断によって会合が崩されることで低粘度になると考えられる。今回の光ピンセットによる測定で，PEG 分散水でも擬塑性流体特有の粘度低下を測定できることが明らかとなった。

Figure 5 は Figure 4 に示した光ピンセットで測定した微粒子移動速度が 2.2μm/s(2.2μm/s OP)の時と 6.7μm/s(6.7μm/s OP)時の結果を，横軸を濃度，縦軸を粘度としたもので，さらにキャノン・フェンスケ粘度計により測定した粘度(CF)を加えている。この図から，CNF 分散水と同様に光ピンセットでの測定粘度がキャノン・フェンスケ粘度計での測定粘度より大きく，低速度で粘度が大きくなる傾向が認められた。また同

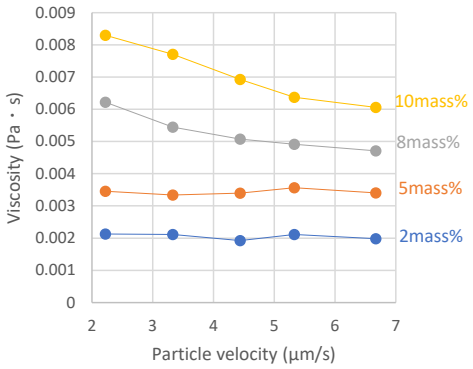

Fig 4. Viscosities of the PEG water dispersions as a function of the particle velocity with the various PEG concentrations between 2 and 10mass%

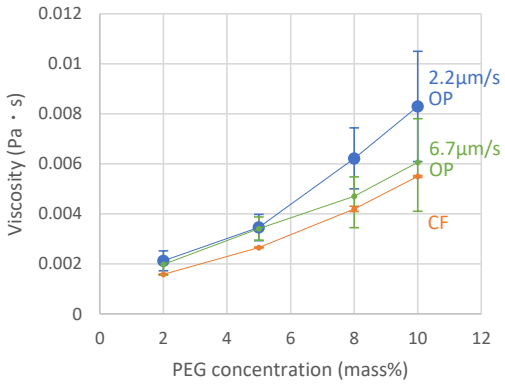

Fig 5. Viscosities of the PEG water dispersions as a function of the PEG concentrations measured by the optical tweezers at the particle velocity of 2.2 and 6.7 μm/s, and the Cannon-Fenske viscometer.

じ濃度であればエラーバーの幅もほぼ同じであり，やはり PEG 濃度の濃淡が存在しているためと思われる。

今回の実験で光ピンセットでもキャノン・フェンスケ粘度計でも見られた傾向として，CNF 分散水と PEG 分散水が同じ粘度になるのに CNF 分散水の方が，圧倒的に濃度が低かった。これは, CNF の長さはサブミクロンサイズで長くさらに水素結合による網目構造によって増粘効果が高く, 対して PEG は今回の実験では式量 8000 のもので重合度が 200 以下と CNF と比べてかなり長さが短く, 増粘効果が小さいためと思われる。

一方，光ピンセットでの粘度測定で特異なことも見られた。CNF 分散水ではキャノン・フェンスケ粘度計の測定値よりも速いせん断速度でも 2 倍以上の粘度で測定された。これは, CNF 分散水は増粘効果が高く, その分だけせん断速度の影響が強く, 光ピンセットで粘度がより大きく測定されたと思われる。対して PEG 分散水ではせん断の効果が小さく, 光ピンセットでもせん断速度が速い場合は, キャノン・フェンスケ粘度計の粘度に近い値になったと思われる。さらにエラーバーの幅は(Figure 3 および Figure 5)は PEG 分散水の方が大きくなっている。粘度が大きいほどその領域の濃度が高いと思われるが, PEG 分散水の濃度差が CNF 分散水のそれよりも大きくなっているためと思われる。このように光ピンセットで CNF 分散水と PEG 分散水の濃度測定傾向の相違についても測定できている。

5. 結言

本研究で光ピンセットを用いて擬塑性の分散水である CNF 分散水と PEG 分散水の粘度を測定した。その結果，分散水濃度が高いほど粘度が高くなり，また擬塑性流体の特徴である微粒子移動速度が速いほど粘度が小さくなることが測定できた。さらにキャノン・フェンスケ粘度計で測定した値よりも光ピンセットで測定した粘度は大きく測定された。加えて CNF 分散水と PEG 分散水の相違についても詳細に測定できた。これらは CNF と PEG の構造や分散水中での相互作用の相違から生じたものと思われる。このように本実験の結果から，光ピンセットで擬塑性の液体の微小領域における粘度を詳細に測定できることが示された。

参考文献

1) 後居 洋介,*粉砕*. 2019, *62*, 39–43.
2) 南井 宣明, 友田 敬二,*色材協会誌*. **1993**, *66*, 434–444.
3) 小野木 重治,*高分子*. **1971**, *29*, 299, 254-266.
4) Matsumoto, N., Maeda, M., Kajita, K., Omiya, Y., Kinoshita, H, *Tribology Online*. **2020**, 15, 68–77.
5) Kinoshita, H., Nishina, Y., Alias, A.A., Fujii, M., ***Carbon***. 2014, *66*, 720–723.
6) Kinoshita, H., Nishina, Y., *Tribology Online*. **2016**, *11*, 235–241.
7) Alias, A.A., Kinoshita, H., Fujii, M.. *Journal of Advanced Mechanical Design, Systems, and Manufacturing*. **2015**, *9*, Paper No.14-00401.
8) 小松 直樹,*表面科学*. **2009**, 30, 273–278.
9) 宮田 完二郎, 長田 健介, 片岡 一則, *Drug Delivery Ssystem*. **2016**, *31*, 283–292.
10) Takahashi, T., Nakamura, H., Kimura, H, *日本機械学会論文集*. **2017**, 83, 16-00560-16–00560.
11) 吉川 史郎, 島崎 泰, *化学工学論文集*. **2014**, *34*, 1, 523–524.
12) 齊藤 利幸, 南里 浩太, 鈴木 健介, 杉浦 忠雄, 松本 直浩, 木之下 博, *材料技術*. **2019**, *38*, 1–8.
13) 春木 直人, *岡山大学大学院自然科学研究科 博士論文*, **1998**.
14) 後居 洋介, 齋藤 継之, 磯貝 明, *Journal of Fiber Science and Technology*. **2018**, *74*, 1, 24–29.
15) Sarkar, A., Ghosh, K., *Kolloid-Zeitschrift & Zeitschrift für Polymere*. **1970**, 236, 2, 140–142.

材料技術の最初のオンライン版（2021 年，第 39 巻，第 1 号）を公開いたしました。公開が遅くなり申し訳ございませんでした。第２号以降についても随時オンライン公開していく予定です。印刷版（第１号～第６号の統合版）の発行は年度末（２０２１年１２月）となりますが，オンライン版については，昨年度以上に掲載決定までの期間の短縮に努めます（２０２０年度については受け取り日から掲載決定までの平均が５４日でした）。奮って御投稿いただけますようお願い申し上げます。

（浜松医科大学　三浦康弘）

MATERIAL TECHNOLOGY 材料技術

昭和62年8月5日第三種郵便物許可　令和３年2月25日発行（隔月25日発行）　第39巻　第１号
定価2,100円